Improving Stiffness, Strength, and Toughness of Poly(omega-pentadecalactone) Fibers through in Situ Reinforcement with a Vanillic Acid-Based Thermotropic Liquid Crystalline Polyester

Wilsens, Carolus H. R. M.; Pepels, Mark P. F.; Spoelstra, Anne B.; Portale, Giuseppe; Auhl, Dietmar; Deshmukh, Yogesh S.; Harings, Jules A. W.

Published in:
Macromolecules

DOI:
10.1021/acs.macromol.5b02419

Publication date:
2016

Macromolecules

Article

pubs.acs.org/Macromolecules

Improving Stiffness, Strength, and Toughness of Poly(ω-pentadecalactone) Fibers through *in Situ* Reinforcement with a Vanillic Acid-Based Thermotropic Liquid Crystalline Polyester

Carolus H. R. M. Wilsens,*[,†] Mark P. F. Pepels,[‡] Anne B. Spoelstra,[‡] Giuseppe Portale,[§] Dietmar Auhl,[†] Yogesh S. Deshmukh,[†] and Jules A. W. Harings[†]

[†]Department of Biobased Materials, Maastricht University, P.O. Box 616, 6200MD Maastricht, The Netherlands

[‡]Laboratory of Polymer Materials, Eindhoven University of Technology, Den Dolech 2, 5600MB Eindhoven, The Netherlands

[§]Macromolecular Chemistry & New Polymeric Materials, Zernike Institute for Advanced Materials, Nijenborgh 4, 9747 AG Groningen, The Netherlands

Supporting Information

ABSTRACT: We report on the morphology and performance of melt-drawn poly(ω-pentadecalactone) (PPDL) fibers reinforced with a vanillic acid-based thermotropic liquid crystalline polyester (LCP). The *in situ* reinforced PPDL/LCP fibers developed in this work are considered to be renewable in nature, given the fact that the feedstock for both polymers can be obtained from natural resources. To prepare these fibers, the polymers were mixed in a small scale twin-screw extruder, followed by melt-drawing of the extrudate. It is demonstrated that the tensile modulus and tensile strength of the fibers increase with increasing LCP orientation and concentration. Despite the brittle nature of the pure LCP component, melt-spun PPDL/LCP fibers maintain their ductile deformation for fibers containing up to 30 wt % LCP. The improved stiffness and strength of these PPDL/LCP fibers in combination with their ductile nature ensure improved energy absorption during deformation and effectively increases their toughness compared to the pure PPDL material. A further increase of the LCP content to 40 wt % and higher results in a poor control over the blend morphology, and brittle failure of the fibers is observed after the application of 2−3% strain. Small-angle X-ray scattering data indicate that after processing transcrystallization of PPDL occurs on the surface of the oriented LCP phase. According to DSC analysis, this transcrystallization on the oriented LCP fibrils is accompanied by an increase in the crystallization temperature. These findings have been confirmed through morphological analysis using transmission electron microscopy. It is anticipated that this interfacial crystallization strengthens the PPDL/LCP interface and allows delocalization of stress during deformation.

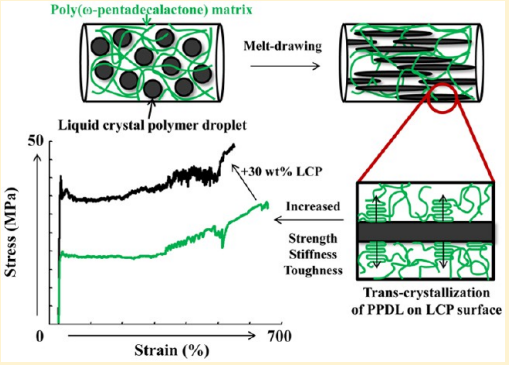

INTRODUCTION

Over the past decade, mankind's interest in polymers from renewable and therefore sustainable resources has increased significantly. Especially renewable polyesters seem to be a class of materials that provide the desired properties to replace commonly used plastics. A recent example of such a material includes poly(ethylene 2,5-furandicarboxylate) as replacement for poly(ethylene terephthalate).[1,2] The renewable aromatic monomer 2,5-furandicarboxylic acid can, for example, be obtained from fructose or produced via the intermediate precursor 5-(hydroxymethyl)furfural.[3−7] Examples of aliphatic biopolyesters include poly(lactic acid) for biomedical and commodity bioplastic applications or aliphatic long-chain polyesters (ALCP) as replacement for polyethylene-like materials.[8−10] The monomers used for the development of ALCPs can generally be obtained from fatty acids, for example, from renewable vegetable oils.[11−14] As has been described by the groups of Gross and Duchateau, the ALCP poly(ω-pentadecalactone) (PPDL) is generally considered a mimic for polyethylene (PE) due to its similarity in crystallization behavior,[15] crystal structure,[16] and mechanical performance.[17,18] The properties of ALCPs can easily be tailored through copolymerization[19] or transesterification reactions[20,21] or through a variation in polymer architecture.[22] Furthermore, the presence of ester groups makes ALCPs good candidates to enhance compatibility, miscibility, nucleation, and/or mechanical performance in blends with other polyesters.[23]

As has already been reported several decades ago, liquid crystal polymers (LCP) are excellent candidates to improve the processing and performance of thermoplastic polymers through melt blending.[24−29] For example, a fine dispersion of LCP fibrils in a thermoplastic matrix is known to improve the

Received: November 6, 2015
Revised: January 31, 2016
Published: March 9, 2016

DOI: 10.1021/acs.macromol.5b02419
Macromolecules 2016, 49, 2228−2237

mechanical performance,[30−32] provide nucleation sites for the matrix material,[33] reduce the viscosity during processing,[34,35] and enhance the heat distortion temperature.[36] It should be noted that although LCP reinforcement is well-known for its improvement of stiffness and strength of polymers, LCP reinforcement generally is accompanied by a decrease in strain at break of the thermoplastic matrix.[28,30,37,38]

Recently, our research group has reported a range of new aliphatic−aromatic LCPs having low melting temperatures and broad processing windows.[39] These materials, obtained from sugar or lignin derived monomers, could readily be processed into fibers having tensile moduli around 10 GPa.[40] Furthermore, since their melting temperatures lie well below 200 °C, these materials are interesting candidates for blending with ALCPs such as PPDL at mild processing temperatures, thereby limiting transesterification and degradation reactions.

To demonstrate that there can be significant synergy between these renewable polyesters, in this study we report on the blending, fiber spinning, and the increase in tensile strength, tensile modulus, and toughness of renewable PPDL/LCP blends.

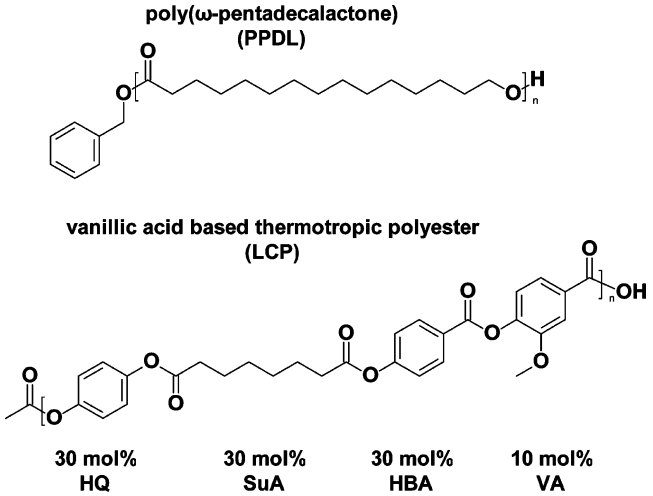

Figure 1. Chemical structures of the polymers used for the blending and melt-drawing experiments performed in this study. N.b.: the vanillic acid-based LCP is a random copolymer.[39]

EXPERIMENTAL SECTION

Material Preparation. Poly(ω-pentadecalactone) (PPDL) synthesis was performed in a 10 L double-wall stainless-steel reactor equipped with a mechanical spiral stirrer. The reactor was dried by heating at 40 °C *in vacuo* for 6 h prior to use. Subsequently, the reactor temperature was increased to 100 °C, and ω-pentadecalactone (PDL) (2.5 kg, 10.4 mol) was added and degassed under vacuum for 1 h, after which 5 L of dry toluene was added under a nitrogen atmosphere. A catalyst solution was prepared in a 250 mL round bottomed flask by the reaction of $Al(Et)_3$ (3.0 g, 26 mmol) and *N*,*N*′-ethylenebis(salicylimine) (salen, 7.0 g, 26 mmol) in 150 mL of toluene for 60 min at 100 °C under an argon-rich atmosphere. Subsequently, benzyl alcohol (2.8 g, 26 mmol) was added to the solution, which was allowed to react for an additional 60 min, thereby *in situ* generating [salen]Al(OBn).[41] The catalyst solution was transferred into the reactor, and the reaction was allowed to proceed for 40 h at 100 °C. Next, the reaction mixture was taken out of the reactor, cooled with liquid nitrogen, and grinded into granules. These granules were subsequently washed 3 times with 10 L of methanol. Next, an acetone solution containing antioxidants Irganox 1010 and Irgafos 168 (0.5 wt % each relative to PPDL) was added. Subsequently, the acetone was allowed to evaporate under air, after which the granules were dried under vacuum yielding 2.1 kg of PPDL. The PPDL was obtained with an M_w of 98 kg/mol and a polydispersity (M_w/M_n) of 2.1, according to high-temperature SEC analysis (160 °C, 1,2,4-trichlorobenzene) calibrated with polyethylene standards (Polymer Laboratories).[42] More details regarding the PPDL are found in a previous publication.[18]

The vanillic acid-based LCP was synthesized on a 200 g scale through a melt-acidolysis copolymerization of acetylated *p*-hydroxybenzoic acid (HBA), vanillic acid (VA), suberic acid (SuA), and hydroquinone (HQ). After loading the monomers together with 100 mg of $Zn(AcO)_2$ in a 500 mL three-neck round-bottom flask fitted with a mechanical stirrer, the temperature was slowly increased to 260 °C. Reduced pressure was applied for 12 h after collecting 90% of the theoretic amount of acetic acid. The polymer was isolated after cooling and grinding the material. The polymer exhibited a melting temperature of 127 °C and was obtained with a weight-average molecular weight, M_w, of 44 kg/mol and a polydispersity (M_w/M_n) of 2.6, according to analysis via size-exclusion chromatography with 1,1,1,3,3,3-hexafluoro-2-propanol as eluent.[40] Figure 1 shows the chemical structures of the polymers used in this study.

Blending and Melt-Drawing Process. PPDL and LCP were dried overnight *in vacuo* at 80 °C prior to extrusion. Mixtures containing 6 g of polymer were weighed and fed into a small-scale DSM Xplore MC15 twin-screw extruder via a water-cooled hopper. The polymers were loaded and processed under a nitrogen-rich flow to prevent degradation and side reactions. All samples were mixed at a rotational speed of 100 rpm for 10 min at 180 °C. Melt-spun fibers were obtained through melt-drawing of the extruded blend, quenching in a water bath, and winding on a bobbin having a diameter of 10 cm. The take-up speed of the bobbin was slowly increased to improve the draw ratio of the fibers. The draw ratio of the quenched fibers was calculated by dividing the diameter of the extruder outlet by the diameter of the fibers. The diameter of the fiber was calculated using fiber length, mass, and density. Fibers were tested without further drying, postprocessing, or recrystallization, unless stated otherwise.

Characterization Methods. The peak melting temperature (T_m) and peak crystallization temperature (T_c) and their corresponding enthalpies (ΔH_m and ΔH_c) were determined by differential scanning calorimetry (DSC) using a TA Instruments Q1000 DSC. All heating and cooling rates were performed at 10 °C/min, unless stated otherwise, while keeping the sample pans under a nitrogen-rich atmosphere. To prevent heat transfer effects on the peak positions, sample weights of 2.0 ± 0.2 mg were adopted to ensure repeatable determination of the T_m and T_c.

Tensile test experiments were performed on a Zwick 100 tensile instrument using a 100 N load cell. Fibers having variable diameters and a fiber length of 20 mm were tested at ambient conditions and constant deformation rate of 5 mm/min. Fiber measurements resulting in breakage at the clamp position were discarded to ensure repeatability of the tensile tests and conclusive results.

2D small-angle X-ray scattering (SAXS) patterns were taken at the DUBBLE beamline (BM26B) at the European Synchrotron Radiation Facility (ESRF) in Grenoble, France, particularly optimized for polymer science, as has been reported by Bras and co-workers[43] and Portale and co-workers.[44] Samples were placed in a Linkam CSS-450 shear cell, which was in turn placed in the X-ray beam. The wavelength of the X-ray photons was 0.1 nm. Samples were irradiated, and SAXS images were collected with a Pilatus 1M detector (169 mm × 179 mm active area) placed at 6 m distance from the sample. The modulus of the scattering vector *q*-scale was calibrated using the position from diffraction peaks of a standard rat tail tendon collagen fiber, where $q = 4\pi \sin\theta/\lambda$ with θ being half of the scattering angle. All samples were heated and cooled at a rate of 10 °C/min to the desired temperature. Samples were measured under quiescent conditions or were subjected to shear during an isothermal period, prior to following the crystallization process during cooling to room temperature at a rate of 10 °C/min. The maximum value in the Lorentz-corrected 1D WAXS pattern was identified as the long period (L_p) of the samples. The Lorentz correction has been applied through multiplying the measured intensity distribution by a factor q^2.

DOI: 10.1021/acs.macromol.5b02419
Macromolecules 2016, 49, 2228−2237

Scanning electron microscopy (SEM) was performed on a JEOL 7500 FA setup. The images showing the morphology of the samples were collected at a voltage of 5−10 kV. Prior to SEM analysis, the samples were cryogenically fractured and pasted on a sample holder using conductive carbon tape. A thin gold coating was applied on the samples through a sputter-coating process. For the analysis of the fibers after yielding, no cryogenic fracture was performed, but instead these samples were prepared using cryomicrotomy, prior to the application of the conductive coating.

Transmission electron microscopy (TEM) analysis was performed using the following procedure. Before analysis, samples were cut into small sections (trimmed at −100 °C) and subsequently stained for 20 h in a RuO_4 solution, according to the procedure described by Montezinos and co-workers.[45] Because of their thin diameter, the melt-spun fibers were not trimmed but were directly placed in the staining solution for 20 h. After staining the amorphous PPDL phase, the samples were cut at −100 °C into thin sections of ∼70 nm thickness using a Leica Ultracut S/FCS microtome. The sections were examined using a Tecnai 20 TEM, operated at 200 kV, after placing them on a 200 mesh copper grid with a carbon support layer. To evaluate the effect of slow crystallization of the PPDL phase, recrystallized samples were prepared and analyzed using TEM analysis. In order to prepare these recrystallized fibers, the as-spun fibers were (1) gradually heated at a rate of 10 °C/min to 110 °C to melt the PPDL phase, (2) kept isothermal for 5 min, and (3) cooled back to room temperature at a rate of 10 °C/min, prior to the TEM sample preparation process.

RESULTS AND DISCUSSION

Thermal Behavior and Morphology of PPDL/LCP Blends. Since the aim of this study is to probe the compatibility and synergy of pure PPDL and LCP materials after extrusion and consecutive fiber spinning, no additional transesterification catalysts or surface agents were added to enhance the blend compatibility and morphology. Preliminary GPC studies were performed to probe the degree of transesterification occurring during the blending process. However, no common solvent was found for the PPDL/LCP blends, preventing accurate GPC analysis. Instead, transesterification between aromatic and aliphatic model compounds was probed in a reaction between butyl hexanoate (0.5 g, 2.9 mmol), phenyl benzoate (0.575 g, 2.9 mmol), and 1-pentadecanol (7 mg, 0.029 mmol). These compounds were added to a crimp cap vial under a nitrogen atmosphere (MBraun MB-150 GI glovebox), capped, taken out of the glovebox, and placed in a salt bath at 180 °C. After 40 min, an aliquot was taken and revealed no exchange of the aliphatic/aromatic ester groups according to ^{1}H NMR and gas chromatography analysis. Similarly, the catalyst, as used during polymerization of the LCP, showed no activity under these conditions. This indicates that it is unlikely that compatibilization of the PPDL/LCP blend occurs through transesterification during the blending process due to the absence of an active catalyst.

To evaluate the dispersion of the blends, scanning electron microscopy (SEM) was performed on cryogenic fracture surfaces of both the nonoriented extrudates and the melt-drawn fibers. Figure 2 shows the characteristic morphology of PPDL and a PPDL/LCP 80/20 blend after processing. No variation in morphology is observed for pure PPDL after extrusion (Figure 2A) or after melt-drawing (Figure 2C). For the extruded PPDL/LCP samples, a LCP droplet dispersion with a particle diameter of 1.9 ± 0.4 μm (averaged over 50 particles) is observed in the PPDL matrix, as is shown in Figure 2B. These droplets deform during the melt-drawing process

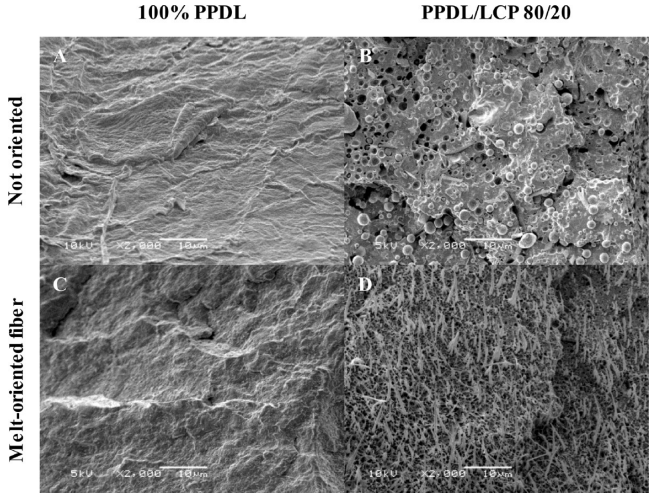

Figure 2. Morphology as observed with SEM after blending and extrusion of (A) PPDL, (B) PPDL/LCP 80/20 blend, (C) PPDL after melt drawing, and (D) PPDL/LCP 80/20 after melt-drawing (draw-ratio of 400). The analyzed plane of the melt-oriented fibers (C) and (D) is perpendicular to the drawing direction of the fibers.

into microfibrils having a diameter at the center of 0.74 ± 0.18 μm and an estimated fibril length of approximately 16.8 ± 5.9 μm. These values are an average of 25 fibrils in fibers with a draw rate of 400 (Figure 2D and Figure S1 from the Supporting Information). The total fibril length was estimated from the SEM images by multiplying the distance between the center diameter and end of the fibril by a factor 2, assuming the fibril diameter is largest at the center of the fibril. Combination of these values yields an average L/D ratio close to 23. It should be noted that the L/D ratio is dependent on the draw ratio of the fiber, and thus higher L/D ratios can be expected for fibers with increasing draw ratio.

The LCP droplet size and dispersion increases significantly and becomes highly irregular for samples having an LCP content of 40 wt %. For example, in oriented PPDL/LCP 60/40 fibers, fibrils having diameters varying from 2 to more than 10 μm are observed. The SEM figures showing the morphology of the PPDL/LCP 60/40 fibers are supplied in the Supporting Information in Figure S1. Since the dispersion of these LCP fibrils could not be controlled without the addition of compatibilizers, no blends with LCP contents higher than 40 wt % were prepared.

DSC analysis was performed on both the as-extruded blends and the melt-drawn fibers to probe the effect of the LCP phase on the crystallization behavior of PPDL. All samples were heated from room temperature up to a maximum temperature of 200 °C at a rate of 10 °C/min. As is visible from Table 1 for the as-extruded blends, the PPDL phase exhibits a peak melting (T_m) and crystallization (T_c) temperature around ∼94−98 and 80 °C, respectively. Furthermore, both the T_m and T_c of PPDL are independent of the LCP concentration present in the blends and the enthalpy of these transitions correlate linearly to the total PPDL content. This implies that the LCP and PPDL phases are not miscible, and no dissolution of LCP occurs in the PPDL matrix during blending. Furthermore, the DSC data indicate that the surface created by the dispersed nonoriented LCP droplets does not influence the melting and crystallization temperatures of the PPDL phase.

In contrast, a clear shift in the T_c of PPDL is observed in DSC analysis of the melt-drawn fibers, but only when the LCP

DOI: 10.1021/acs.macromol.5b02419
Macromolecules 2016, 49, 2228−2237

Table 1. Overview of the DSC Data of the Extruded Blends, Obtained from the Second Heating and Cooling Cycle[a]

composition (wt %)		second cycle			
PPDL	LCP	T_m[b] (°C)	ΔH_m (J/g)	T_c[b] (°C)	ΔH_c (J/g)
100	0	97.0	118.9	80.7	110.5
90	10	98.6	114.6	79.4	106.1
80	20	93.9	99.0	80.9	92.5
70	30	96.5	87.6	79.3	83.4
60	40	93.5	78.5	80.3	74.4
0	100	126.5	1.8	90.1	0.94

[a]The heating and cooling cycles were performed between 20 and 200 °C at a rate of 10 °C/min. [b]The T_m and T_c transitions correspond to transitions of the PPDL phase of the blend. For the PPDL/LCP 0/100 material, the T_m and T_c reflect the transitions of the pure LCP material.

fibrils are not molten during the heating ramp. For example, a shift in T_c of PPDL of roughly 2 °C is observed upon cooling when the PPDL/LCP fibers are heated only up to 110 °C, a temperature where the LCP fibrils remain in the semicrystalline state (T_m = 127 °C). To illustrate, Figure 3 shows the second heating and cooling run in the temperature range between 70 and 100 °C (maximum temperature in the DSC run was 110 °C) of a PPDL fiber, a PPDL/LCP 80/20 fiber, and a PPDL/LCP 80/20 fiber where the LCP fibrils were heated to 200 °C prior to the DSC experiment. From Figure 3 it can be seen that the pure PPDL fiber shows a T_c at 80.6 °C, which is in good agreement with the values presented in Table 1. In contrast, the PPDL/LCP 80/20 fiber exhibits a T_c of 82.4 °C (±0.17 °C, based on three experiments). A similar shift in crystallization temperature is observed during DSC analysis of fibers with other LCP loadings. For example, at a cooling rate of 10 °C/min, for a PPDL/LCP 60/40 fiber, a T_c of 82.3 °C is observed.

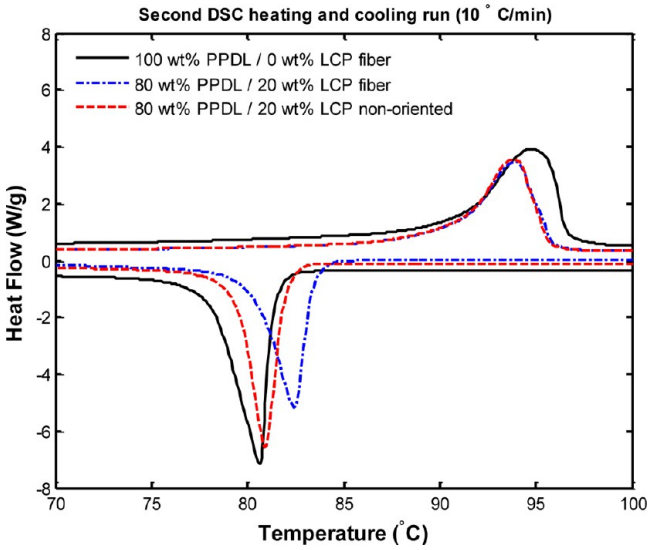

Figure 3. Characteristic DSC heating and cooling run (second cycle) depicting the melting and crystallization behavior of a pure PPDL fiber (ΔH_c = 113.2 J/g), a PPDL/LCP 80/20 fiber where the LCP phase is molten and contracted into nonoriented droplets after heating to 200 °C (ΔH_c = 94.3 J/g), and PPDL/LCP 80/20 fiber where the LCP phase is dispersed as oriented fibrils (ΔH_c = 92.7 J/g). The maximum temperature programmed in this run was set to 110 °C to ensure the LCP phase did not melt during the experiment.

For illustrative purposes, DSC cooling traces taken at 1 °C/min, showing the clear shift in the crystallization transition, are supplied in Figure S2.

No significant nucleation effect is observed upon cooling the fibers when they have been heated to 200 °C, as is visible from Figure 3. Under these conditions, the LCP fibrils melt and contract into nonoriented droplets during the heating ramp, yielding T_c values comparable to the data presented in Table 1. To note, the enthalpy of the crystallization transition does not change when performing the DSC run up to 200 °C or up to 110 °C; only the peak crystallization temperature and onset of crystallization shift. This indicates that the presence of the LCP likely affects the nucleation of the PPDL phase but does not seem to influence the crystallinity of the PPDL phase.

Overall, the combined data shown in Table 1 and Figure 3 demonstrate that the PPDL crystallization is only enhanced when the fibrillary morphology of the LCP phase, as induced by the fiber-spinning process, is not destroyed during the heating ramp. When LCP fibrils are molten, the fibrillary LCP morphology generated during the spinning process is lost, and no enhanced PPDL crystallization is observed upon cooling. To probe the origin of this nucleation effect of the PPDL phase in the as-spun fibers, in the next section we report on the morphology of the PPDL/LCP fibers obtained after various crystallization conditions.

Morphology in Oriented PPDL/LCP Blends. Small-angle X-ray scattering (SAXS) was performed at various temperatures on as-spun PPDL/LCP fibers under both quiescent conditions and after the application of shear. As is visible from Figure 4A, the melt-drawn PPDL fibers show an isotropic scattering signal, corresponding to a random distribution of the PPDL crystals. This indicates that for pure PPDL fibers, any orientation induced during the spinning process has completely relaxed upon crystallization of the fiber during cooling. In general, the long period (L_p) obtained for the as-spun PPDL fibers lies around ~14 nm, which is likely a result from the quenching of the fiber during the spinning process: As a result from the rapid cooling of the as-spun materials, the PPDL phase is subjected to a large undercooling which generally results in a decrease in both the lamellar thickness and crystallinity (hence a lowered L_p) compared to samples that are allowed to crystallize slowly. Upon melting of the PPDL matrix (>95 °C), loss of the isotropic scattering signal is observed. Similar to the as-spun fiber, cooling back to room temperature at a rate of 10 °C/min results in isotropic crystallization of the PPDL sample and, as expected from the slow cooling rate, results in an increase of the L_p to 21.3 nm.

As is depicted in Figure 2D, the spinning process results in orientation of the LCP droplets into fibrils. Although LCP fibrils can have high molecular orientation, the absence of systematic long-range order in the nematic phase generally prevents well-defined SAXS signals. However, during processing of rigid-rod polymers, voids or oriented crystals can be formed.[46,47] These crystals or voids are stretched along the fiber drawing direction, resulting in the observation of streaks of scattering intensity in the 2D SAXS images, located perpendicular to the fiber *c*-axis. As is visible from Figure 4B, such streaks of scattering intensity are present in melt-drawn PPDL/LCP fibers, confirming that the LCP phase is molecularly oriented during the melt-drawing process.

Interestingly, in the melt-spun fibers, the PPDL crystals grow perpendicular to the LCP fibrils. This is indicated by the lobe-like scattering signals found along the vertical/fiber axis in

DOI: 10.1021/acs.macromol.5b02419
Macromolecules 2016, 49, 2228−2237

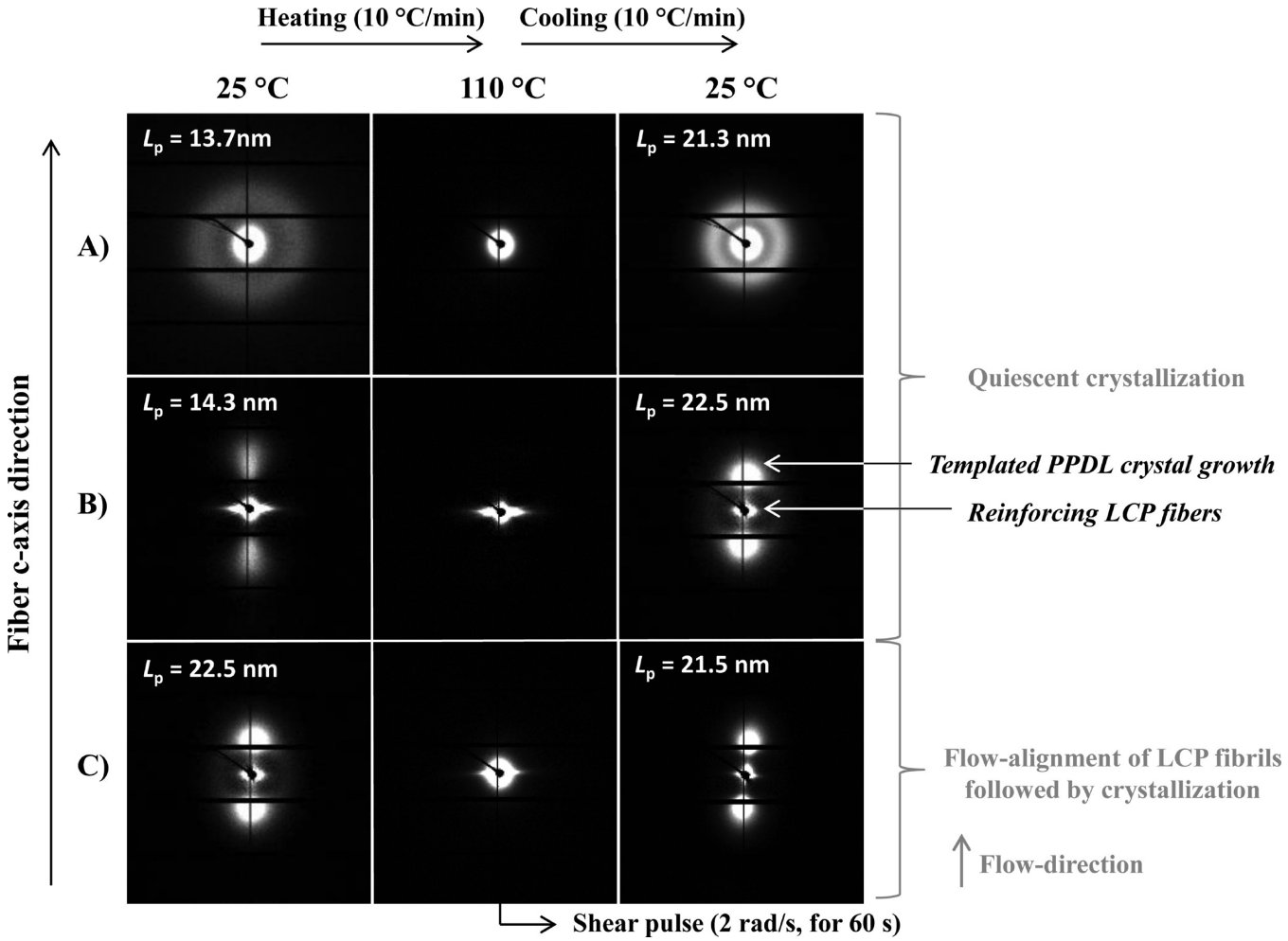

Figure 4. 2D SAXS patterns of melt-drawn fibers taken at 25 °C, after heating to 110 °C (10 °C/min), and after consequent cooling back to 25 °C (10 °C/min). (A) Pure PPDL, (B) PPDL/LCP 80/20 fiber bundle, (C) second heating and cooling run of sample B, where a shear pulse of 2 rad/s for 60 s is applied at 110 °C, prior to cooling. For all SAXS images shown in this figure, the fibers were placed with their drawing direction vertically with respect to the detector images. Values for the long period (L_p) calculated from the SAXS data are embedded in the 2D SAXS images. An example of the obtained Lorentz-corrected intensity profiles is supplied in Figure S3.

Figure 4B: the vertical positioning of the scattering signal originates from PPDL crystal lamellae growing perpendicular to the draw direction of the fiber, thereby having the crystal lamellae periodically ordered along the draw direction. As has been described by the groups of Fu[48] and Peters,[49] such characteristic scattering patterns in semicrystalline polymers are generally associated with transcrystallization or (hybrid) shish-kebab crystallization morphologies. Since the SAXS data provide no indication for the presence of daughter lamella,[50] we expect that the morphology observed in the PPDL/LCP fibers is a result from transcrystallization of PPDL on the surface of the oriented LCP phase.[51] To note, the L_p of the PPDL phase does not change significantly after crystallization in the presence of LCP fibrils; upon cooling at a rate of 10 °C/min, a L_p of 22.5 nm is observed for the crystalline phase at room temperature.

The transcrystallization of PPDL on the surface of the LCP fibrils is regained after heating the fibers to 110 °C, followed by cooling and recrystallization of the PPDL phase (Figure 4B). Furthermore, the application of shear at 110 °C in PPDL/LCP systems results in flow alignment of the LCP fibrils and a further orientation of the PPDL crystals perpendicular to the shearing direction after recrystallization (Figure 4C). This data indicates that the PPDL/LCP fibers can be reprocessed with re-establishment of PPDL transcrystallization, as long as the LCP fibrils remain in their oriented state. The oriented PPDL crystal growth is lost when the LCP fibrils are heated beyond their melting temperature: only isotropic PPDL crystallization is observed upon cooling, with and without the application of shear prior to cooling.

To confirm the transcrystallization of PPDL occurring on top of the oriented LCP fibrils, transmission electron microscopy (TEM) analysis was performed on samples containing both nonoriented LCP droplets and oriented LCP fibrils. During the staining procedure of the samples the RuO_4 diffuses selectively into the amorphous phase of PPDL, providing strong contrast due to the heavy element Ru. The crystal lamellae appear as white lines in the TEM figures, and the line widths correspond to the thickness of lamellae.[45] Since the LCP phase proved to be less affected by the staining method and does not have a well-defined crystal morphology, LCP droplets or fibrils are detected as gray areas. As is visible from Figure 5, pure semicrystalline PPDL contains a random distribution of chain-folded crystals. For the as-extruded PPDL/LCP samples it is observed that lamellae grow both perpendicular and parallel to the LCP droplet surface. This indicates that though

DOI: 10.1021/acs.macromol.5b02419
Macromolecules 2016, 49, 2228−2237

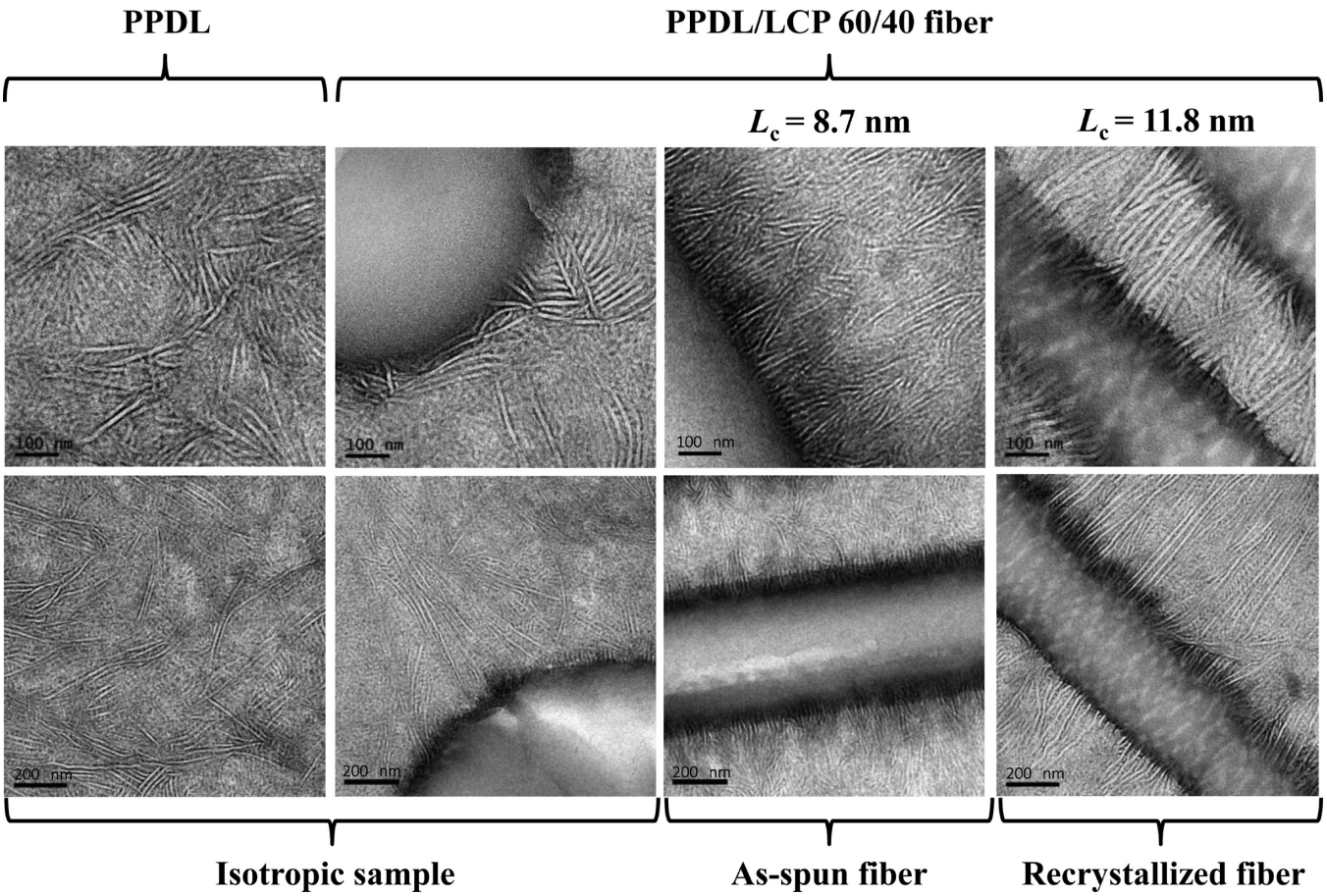

Figure 5. TEM images showing the morphology of PPDL and PPDL/LCP 60/40 blends observed in the isotropic state, the as-spun fiber, and recrystallized fiber (after heating to 110 °C). Values for the lamellar thickness (L_c) of the PPDL crystals in the as-spun and recrystallized fibers are averaged over 20 lamellae.

crystallization of PPDL crystals occurs on the surface of the LCP droplets, they do not exhibit a preferred crystal growth direction.

In contrast, PPDL lamellae have a clear tendency to grow perpendicular to oriented LCP fibrils. As can be seen from the TEM figures of the as-spun fibers in Figure 5, almost all lamellae (having an average lamellar thickness L_c of 8.7 nm) on the LCP fibril surface are located perpendicular to the LCP fibril direction, confirming that transcrystallization is occurring. In these as-spun fibers, it can be seen that the crystal growth direction gradually becomes isotropic further away from the fibril. It is likely that this is a result from the high cooling rate of the fiber during the melt-drawing process. Indeed, both the length and the L_c of the lamella growing on the surface of the LCP fibrils increase drastically when heating the PPDL/LCP fibers to 110 °C, followed by cooling at a rate of 10 °C/min (Figure 5, recrystallized fiber). To reflect, the average lamellar thickness observed from the TEM images for PPDL crystals after cooling at a rate of 10 °C/min increases to ∼11.8 nm. For comparison, the L_c can be approximated from SAXS data using the formula $L_c = L_pX$, where X is the crystallinity of the PPDL phase and L_p is obtained from the SAXS data (∼22 nm). Since determination of the PPDL crystallinity from a WAXD fiber pattern of PPDL/LCP fibers is expected to be inaccurate due to overlap in scattering signals, the crystallinity of the PPDL phase is estimated to be 50% based on previously reported results.[18] From this estimation, a L_c of ∼11 nm is expected for recrystallized samples, which corresponds well with the 11.8 nm observed from TEM analysis. Similarly, the L_c expected from the SAXS data for the as-spun fibers (∼7 nm) is in range with the value of 8.7 nm observed from the TEM data.

Overall, the combined SAXS and TEM data confirm that transcrystallization of PPDL occurs on the surface of the LCP phase. Interestingly, transcrystallization of PPDL occurs predominantly perpendicular to the surface of *oriented* LCP fibrils. Although PPDL crystallization is also detected on the surface of *nonoriented* LCP droplets, no preferred crystal growth direction is observed. Though the exact reason for this selective transcrystallization on the oriented LCP surface is unknown, we anticipate that the alignment of LCP promotes the formation of oriented nonperiodic layer (NPL) crystallites[52] that provide sufficient regularity to act as a nucleation site for PPDL. Please note that other factors such as (1) variations of the geometry and surface roughness of the LCP phase,[48] (2) the orientation, interfacial stresses, and interfacial energies of the (either macroscopically aligned or isotropically distributed) nematic LCP domains at the PPDL/LCP interphase,[53] and (3) the distribution of monomers in the backbone of the LCP chains and the resulting variations in NPL crystallites and total crystallinity of the LCP[39] are also likely to influence the PPDL nucleation.

Tensile Performance of Melt-Drawn PPDL/LCP Fibers. To probe the effects of the LCP reinforcement in the PPDL matrix, the tensile performance of the melt-drawn fibers was evaluated. The as-spun fibers containing 0, 20, 40, and 100 wt % of LCP were evaluated as a function of draw ratio. Since

DOI: 10.1021/acs.macromol.5b02419
Macromolecules 2016, 49, 2228−2237

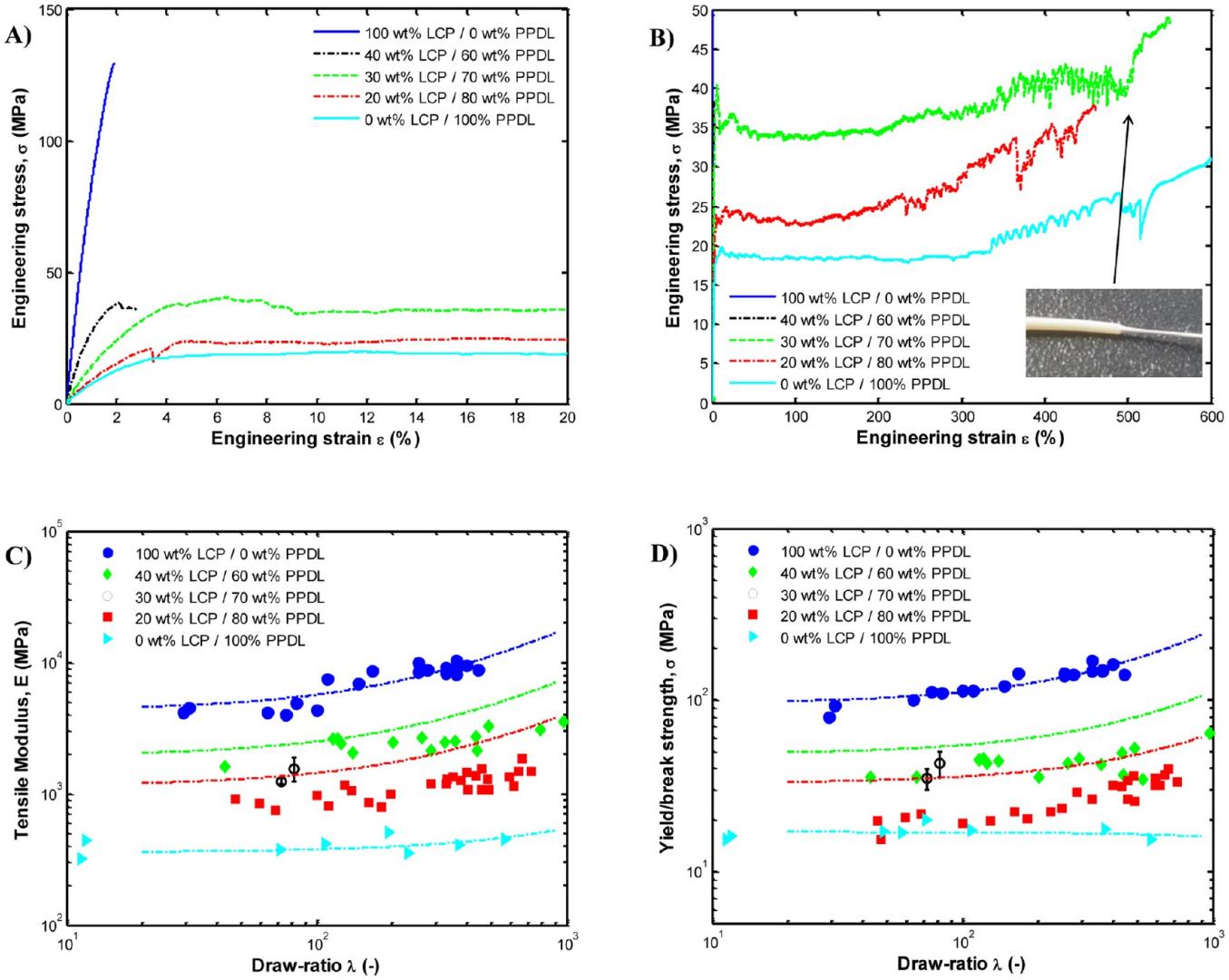

Figure 6. Characteristic tensile performance observed for the as-spun fibers of PPDL, LCP and PPDL/LCP 60/40, 70/30, and 80/20 blends in the range (A) 0−20% strain and (B) 0−600% strain. The inset in (B) shows characteristic neck formation observed during deformation of a 500 μm thick melt-drawn fiber containing 30 wt % LCP and 70 wt % PPDL. (C) and (D) depict the dependency of the tensile modulus and yield strength, respectively, of melt-spun fibers as a function of draw ratio. Fitted data (assuming linear dependency) and predictions according to the linear rule of mixtures are added as dotted lines. Fibers containing 30 wt % LCP were spun under constant speed to determine the deviation of the fiber properties. The standard deviation (average of five fibers) is denoted in error bars for the fibers containing 30 wt % LCP. The data points of the other fibers correspond to single experiment values.

oriented LCP materials generally exhibit high stiffness, high strengths at break, and a low strains at break, we can assume that LCP fibrils act as hard fillers in the PPDL matrix. Since the tensile moduli and strength-to-failure of the pure LCP material increases with increasing molecular orientation, it is expected that the strength to failure and tensile modulus of the *in situ* oriented LCP fibrils also increase with draw ratio of PPDL/LCP fibers. As a result, the tensile modulus of the PPDL/LCP fibers should also increase with increasing LCP orientation and/or LCP concentration. Similarly, the yield stress of the PPDL/LCP fibers should increase with increasing LCP orientation and LCP loading, assuming that the surface interaction between the PPDL and the LCP phase is strong enough to transfer stresses imposed on the PPDL matrix to the LCP fibrils. Since interfacial crystallization generally enhances the interfacial interactions between fillers and semicrystalline polymers,[48] we can expect to see such an enhancement of yield strength in the PPDL/LCP fibers. An overview of the tensile performance of the fibers is shown in Figure 6. Figures 6A and 6B show characteristic tensile curves obtained during tensile testing of the various fibers developed in this study. Figures 6C and 6D show the dependency of the tensile modulus and yield strength of the various fibers as a function of the draw-ratio. Indeed, as anticipated, both the tensile modulus and the yield strength of the PPDL/LCP fibers increase with LCP loading and draw-ratio as is visible from Figure 6.

Although a clear increase in performance is observed for the *in situ* reinforced PPDL/LCP fibers as a function of draw ratio and LCP concentration, the performance is lower than predicted by the linear rule of mixtures: By fitting the dependency of the tensile modulus of the pure fiber materials and by using eq 1, we can predict the optimal modulus of the *in situ* reinforced PPDL/LCP fibers.

$$E_{\text{blend}} = f(E_{\text{LCP}}) + (1 - f)(E_{\text{PPDL}}) \quad (1)$$

DOI: 10.1021/acs.macromol.5b02419
Macromolecules 2016, 49, 2228−2237

In eq 1, E_x corresponds to the modulus of component X, and f corresponds to the weight fraction of LCP. In this calculation, the dependency of the tensile modulus on the draw ratio was assumed to be linear. Both the fitted data and the prediction of the modulus for the blends are shown in Figure 6C as dotted lines. The same approach is adopted to predict the yield strength of the *in situ* reinforced PPDL/LCP fibers. The resulting data fits and predictions are added as dotted lines in Figure 6D.

As is visible from Figure 6C, the tensile modulus of the fibers seems to follow the predicted values quite well, even though the values are slightly lower than predicted. One possibility for the nonoptimal tensile modulus of the PPDL/LCP fibers is a decreased molecular orientation of the LCP fibrils compared to pure LCP fibers spun under the same conditions. To compare the molecular orientation of the LCP phase in pure LCP fibers and PPDL/LCP fibers, wide-angle X-ray diffraction (WAXD) experiments were performed on the single fibers using a Bruker D8 equipped with a 2-dimensional GADDS detector. The obtained 2-dimensional WAXD images were used to determine the azimuthal intensity distribution at the maximum of the LCP interchain diffraction peak (2θ = 21°).[40] Next, following the procedure described by Mitchell and Windle,[54] the orientation parameter $\langle P_{2n}(\cos\ \varphi)\rangle_d$ was calculated by weighting the average Legendre polynomial against the obtained azimuthal intensity scan. Comparison of the obtained orientation parameters $\langle P_{2n}(\cos\ \varphi)\rangle_d$ of the LCP component in fibers (draw ratio of 800) of pure LCP (0.86) and PPDL/LCP 60/40 (0.70) indicates that indeed the LCP phase exhibits a lowered molecular orientation after spinning. However, it should be noted that during the determination of the order parameter of the LCP phase, partial overlap of the interchain diffraction signals of oriented PPDL and LCP structures is observed. This implies that the azimuthal intensity distribution reflects both the orientation of the LCP phase and orientation of the amorphous PPDL phase. Therefore, though we expect that the amorphous phase of PPDL is not oriented during the melt-spinning process, any orientation of the amorphous PPDL phase will influence the obtained orientation parameter. Further information on this subject, the WAXD patterns, and azimuthal density distributions are supplied in the Supporting Information. When ignoring possible contributions from the amorphous PPDL phase, the WAXD data confirm that the LCP phase is not as strongly oriented in PPDL/LCP blends as in pure LCP fibers spun under the same conditions.[40] However, taking the potential inaccuracy of the orientation parameter determination procedure into account, the WAXD data are not conclusive.

Though the tensile modulus of the fibers seems to follow the predictions from the rule of mixtures quite well, the yield strength is significantly lower than predicted, as is visible from Figure 6D. A possible explanation for the mismatch in experimental and predicted yield strength of the fibers is the occurrence of gradual debonding of the PPDL/LCP interface during the deformation applied prior to yielding. As a result, the maximum transferable stress to the LCP fibrils during deformation is limited by the interface interactions and yielding occurs at a spot where fibrils are locally debonded. To identify whether debonding occurs during deformation, SEM characterization was performed on a PPDL/LCP fiber after necking (procedure and data provided in the Supporting Information). Indeed, the SEM images provided in Figure S5 depict voids running along the necked region. Though the SEM images do not allow for differentiation between the LCP and the PPDL phase, it is anticipated that these voids are indeed the result of debonding of the LCP/PPDL interface during deformation.

The fibers containing 40 wt % LCP exhibit brittle deformation behavior and failed after the application of only 2−3% strain, as is visible from Figure 6A. It is expected that this is a result from the poor distribution of the LCP phase as observed earlier during SEM analysis (Figure S1). Since no yielding was observed for the PPDL/LCP 60/40 fibers, the maximum stress prior to failure is presented instead of the yield strength for these fibers in Figure 6D.

In general, necking was observed during deformation of the ductile fibers. Unfortunately, as a result from this necking behavior, the fibers slipped when the neck reached the clamp position (as is detected from Figure 6B as a sudden drop in the tensile curves). For this reason, no accurate values of the true strain at break of these fibers can be supplied. Nonetheless, the fibers containing 20 wt % LCP maintain the macroscopic ductile nature of the PPDL matrix and can be elongated to 500−600% strain and higher prior to failure or slipping from the clamps. To probe whether this ductile deformation persists in samples with 30 wt % LCP, melt-drawing experiments were performed on PPDL/LCP 70/30 blends where fibers were spun under constant draw ratio. The tensile performance of these fibers was evaluated and the standard deviation of both the modulus and the yield stress was determined on an average of five fibers (included in Figure 6). Indeed, similarly to what was observed for fibers containing 20 wt % LCP, fibers containing 30 wt % LCP are of a ductile nature, and clear neck formation is observed after yielding (inset, Figure 6B).

In general, the tensile data of the fibers indicate that the introduction of oriented LCP fibrils into the PPDL matrix improves the tensile modulus and tensile strength, without compromising on the (detectable) strain at break of the fibers. This indicates that the energy absorbed during the deformation prior to failure, hence the toughness of these LCP reinforced PPDL fibers, increases with LCP loading and orientation of the fiber. Taking the PPDL/LCP 70/30 and pure PPDL fibers shown in Figure 6B as example, the inclusion of 30 wt % of LCP results in an approximated 75% increase in toughness compared to the pure PPDL fiber.

Overall, we observe that the mechanical performance of the PPDL/LCP fibers is highly dependent on the spinning conditions, which determine both the molecular orientation and dimensions of the LCP fibrils. For example, increasing draw ratio results in an increase of the LCP fibril orientation and stiffness, but as observed earlier, it also influences the transcrystallization at the PPDL/LCP interface. In turn, this transcrystallization affects the strength of the PPDL/LCP interface which determines the yield strength of the PPDL/LCP fibers. Furthermore, the molecular orientation of the LCP phase affects the strength to failure of the LCP fibrils and therefore governs the maximum yield stress of the PPDL/LCP fibers. Besides, other parameters such as the mixing time, mixing temperature, and cooling rate of the fibers significantly affect the fiber morphology and the distribution of the LCP phase, which in turn affects the mechanical performance. Though it may be clear that the mechanical performance of the PPDL/LCP fibers is complex and dependent on the aforementioned parameters, further enhancement of the tensile modulus, tensile strength, and fiber toughness is expected upon optimizing the processing conditions and LCP dispersion.

DOI: 10.1021/acs.macromol.5b02419
Macromolecules 2016, 49, 2228−2237

CONCLUSIONS

In this study we developed renewable blends of PPDL and vanillic acid-based LCP and reported on their morphology and performance. We have demonstrated that melt-drawn fibers having up to 30 wt % LCP maintain their ductile behavior, while exhibiting an increased tensile modulus and tensile strength. Analysis of the PPDL/LCP interface indicates that transcrystallization of PPDL occurs on the surface of oriented LCP fibrils. We anticipate that the improved mechanical performance of the PPDL/LCP fibers is achieved through the enhancement of the interfacial interactions, resulting from the transcrystallization and the ensuing morphology. Since the mechanical performance of PPDL/LCP fibers is highly dependent on the fiber morphology and processing conditions, we expect a further enhancement in mechanical performance upon optimization of the processing parameters and LCP dispersion. Overall, on the basis of this study, we can conclude that LCP blending is a complex, but promising route to improve the tensile modulus, yield strength, and toughness of ductile aliphatic polyesters.

ASSOCIATED CONTENT

Supporting Information

The Supporting Information is available free of charge on the ACS Publications website at DOI: 10.1021/acs.macromol.5b02419.

Figures S1−S5 (PDF)

AUTHOR INFORMATION

Corresponding Author

*E-mail karel.wilsens@maastrichtuniversity.nl (C.H.R.M.W.).

Notes

The authors declare no competing financial interest.

ACKNOWLEDGMENTS

NWO (Nederlandse Organisatie voor Wetenschappelijk Onderzoek) is acknowledged for providing beam-time at the ESRF. The DUBBLE (Dutch Belgian beamline) staff is acknowledged for supporting the X-ray experiments.

REFERENCES

(1) Burgess, S. K.; Leisen, J. E.; Kraftschik, B. E.; Mubarak, C. R.; Kriegel, R. M.; Koros, W. J. *Macromolecules* **2014**, *47*, 1383−1391.
(2) Gandini, A.; Silvestre, A. J. D.; Neto, C. P.; Sousa, A. F.; Gomes, M. *J. Polym. Sci., Part A: Polym. Chem.* **2009**, *47*, 295−298.
(3) Gandini, A. *Polym. Chem.* **2010**, *1*, 245−251.
(4) Bicker, M.; Hirth, J.; Vogel, H. *Green Chem.* **2003**, *5*, 280−284.
(5) Moreau, C.; Belgacem, M. N.; Gandini, A. *Top. Catal.* **2004**, *385*, 1−13.
(6) Kröger, M.; Prüße, U.; Vorlop, K.-D. *Top. Catal.* **2000**, *13*, 237−242.
(7) Munoz De Diego, C.; Schammel, W. P.; Dam., M. A.; Gruter, G. M. Method for the prepration of 2,5-furandicarboxylic acid and the esters thereof, WO2011043660, 2011.
(8) Lasprilla, A. J. R.; Martinez, G. A. R.; Lunelli, B. H.; Jardini, A. L.; Maciel Filho, R. *Biotechnol. Adv.* **2012**, *30*, 321−328.
(9) Lim, L.-T.; Aurus, R.; Rubino, M. *Prog. Polym. Sci.* **2008**, *33*, 820−852.
(10) Datta, R.; Henry, M. *J. Chem. Technol. Biotechnol.* **2006**, *81*, 1119−1129.
(11) Seo, J.-H.; Lee, S.-M.; Lee, J.; Park, J.-B. *J. Biotechnol.* **2015**, *216*, 158−166.
(12) Goldbach, V.; Roesle, P.; Mecking, S. *ACS Catal.* **2015**, *5*, 5951−5972.
(13) Lu, W.; Ness, J. E.; Xie, W.; Zhang, X.; Minshull, J.; Gross, R. A. *J. Am. Chem. Soc.* **2010**, *132*, 15451−15455.
(14) Jose, J.; Pourfallah, G.; Merkley, D.; Li, S.; Bouzidi, L.; Lopez Leao, A.; Narine, S. S. *Polym. Chem.* **2014**, *5*, 3203−3213.
(15) Skoglund, P.; Fransson, A. *Polymer* **1998**, *39*, 1899−1906.
(16) Gazzano, M.; Malta, V.; Focarete, M. L.; Scandola, M.; Gross, R. A. *J. Polym. Sci., Part B: Polym. Phys.* **2003**, *41*, 1009−1013.
(17) Cai, J.; Liu, C.; Cai, M.; Zhu, J.; Hsiao, B. S.; Gross, R. A. *Polymer* **2010**, *51*, 1088−1099.
(18) Pepels, M. P. F.; Govaert, L. E.; Duchateau, R. *Macromolecules* **2015**, *48* (16), 5845−5854.
(19) Pepels, M. P. F.; Koeken, R. A. C.; van der Linden, S. J. J.; Heise, A.; Duchateau, R. *Macromolecules* **2015**, *48*, 4779−4792.
(20) Todd, R.; Tempelaar, S.; Lo, R. G.; Spinella, S.; McCallum, S. A.; Gross, R. A.; Raquez, J.-M.; Dubois, P. *ACS Macro Lett.* **2015**, *4*, 408−411.
(21) Ceccorulli, G.; Scandola, M.; Kumar, A.; Kalra, B.; Gross, R. A. *Biomacromolecules* **2005**, *6*, 902−907.
(22) Kalra, B.; Kumar, A.; Gross, R. A.; Baiardo, M.; Scandola, M. *Macromolecules* **2004**, *37*, 1243−1250.
(23) Porter, R. S.; Wang, L-H- *Polymer* **1992**, *33*, 2019−2030.
(24) Seo, Y. *J. Appl. Polym. Sci.* **1998**, *70*, 1589−1595.
(25) Chen, L.; Huang, H. Z.; Wang, Y. Z.; Jow, J.; Su, K. *Polymer* **2009**, *50*, 3037−3046.
(26) Grasser, W.; Giesa, R.; Schmidt, H.-W. *Polymer* **2001**, *42*, 8517−8527.
(27) Grasser, W.; Giesa, R.; Schmidt, H.-W. *Polymer* **2001**, *42*, 8529−8540.
(28) Mandal, P. K.; Chakraborty, D. *J. Appl. Polym. Sci.* **2009**, *111*, 2345−2352.
(29) Blizard, K. G.; Baird, D. G. *Polym. Eng. Sci.* **1987**, *27*, 653−662.
(30) Yang, Q.; Hirata, M.; Lu, D.; Nakajima, H.; Kimura, Y. *Biomacromolecules* **2011**, *12*, 354−358.
(31) Saikrasun, S.; Bualek-Limcharoen, S.; Kohjiya, S.; Urayama, K. *J. Appl. Polym. Sci.* **2003**, *90*, 518−524.
(32) Saikrasun, S.; Bualek-Limcharoen, S.; Kohjiya, S.; Urayama, K. *J. Polym. Sci., Part B: Polym. Phys.* **2005**, *43*, 135−144.
(33) Naffakh, M.; Gomez, M. A.; Ellis, G.; Marco, C. *Polym. Eng. Sci.* **2006**, *46*, 1411−1418.
(34) Whitehouse, C.; Lu, X. H.; Goa, P.; Chai, C. K. *Polym. Eng. Sci.* **1997**, *37*, 1944−1958.
(35) Chan, C. K.; Whitehouse, C.; Gao, P.; Chai, C. K. *Polymer* **2001**, *42*, 7847−7856.
(36) Kim, J. Y.; Kang, S. W.; Kim, S. H. *Fibers Polym.* **2006**, *7*, 358−366.
(37) La Mantia, F. P.; Geraci, C.; Vinci, M.; Pedretti, U.; Roggero, A.; Minkova, L. I.; Magagnini, P. L. *J. Appl. Polym. Sci.* **1995**, *58*, 911−921.
(38) Caligiuri, L.; Stagnaro, P.; Valenti, B.; Canalini, G. *Eur. Polym. J.* **2009**, *45*, 217−225.
(39) Wilsens, C. H. R. M.; Verhoeven, J. M. G. A.; Noordover, B. A. J.; Hansens, M. R.; Auhl, D.; Rastogi, S. *Macromolecules* **2014**, *47*, 3306−3316.
(40) Wilsens, C. H. R. M.; Deshmukh, Y. S.; Liu, W.; Noordover, B. A. J.; Yao, Y.; Meijer, H. E. H.; Rastogi, S. *Polymer* **2015**, *60*, 198−206.
(41) Pepels, M. P. F.; Hofman, W. P.; Kleijnen, R.; Spoelstra, A. B.; Koning, C. E.; Goossens, H.; Duchateau, R. *Macromolecules* **2015**, *48*, 6909−6921.
(42) Pepels, M. P. F.; Bouyahyi, M.; Heise, A.; Duchateau, R. *Macromolecules* **2013**, *46*, 4324−4334.
(43) Bras, W.; Dolbnya, I. P.; Detollenaere, D.; van Tol, R.; Malfois, M.; Greaves, G. N.; Ryan, A. J.; Heeley, E. *J. Appl. Crystallogr.* **2003**, *36*, 791−794.
(44) Portale, G.; Cavallo, D.; Alfonso, C.; Hermida-Merino; van Drongelen, M.; Balzano, L.; Peters, G. W. M.; Goossens, G. P. G.; Bras, W. *J. Appl. Crystallogr.* **2013**, *46*, 1681−1689.
(45) Montezinos, D.; Wells, B. G.; Burns, J. L. *J. Polym. Sci., Polym. Lett. Ed.* **1985**, *23*, 421−425.

DOI: 10.1021/acs.macromol.5b02419
Macromolecules 2016, 49, 2228−2237

(46) Chae, H. G.; Kumar, S. *J. Appl. Polym. Sci.* **2006**, *100*, 791−802.
(47) Saw, C. K.; Collins, G.; Menczel, J.; Jaffe, M. *J. Therm. Anal. Calorim.* **2008**, *93*, 175−182.
(48) Ning, N.; Fu, S.; Zhang, W.; Chen, F.; Wang, K.; Denk, H.; Zhang, Q.; Fu, Q. *Prog. Polym. Sci.* **2012**, *37*, 1425−1455.
(49) Troisi, E. M.; Portale, G.; van Drongelen, M.; Hermida-Merino, D.; Peters, G. W. M. *Macromolecules* **2015**, *48*, 2551−2560.
(50) Han, R.; Li, Y.; Wang, Q.; Nie, M. *RSC Adv.* **2014**, *4*, 65035−65043.
(51) Thomason, J. L.; van Rooyen, A. A. *J. Mater. Sci.* **1992**, *27*, 889−986.
(52) Windle, A. H.; Viney, C.; Golombok, R.; Donald, A. M.; Mitchell, G. R. *Faraday Discuss. Chem. Soc.* **1985**, *79*, 55−72.
(53) Thomason, J. L.; van Rooyen, A. A. *J. Mater. Sci.* **1992**, *27*, 897−907.
(54) Mitchell, G. R.; Windle, A. H. In Basset, D. C., Ed.; *Developments in Crystalline Polymers;* Elsevier Applied Science Publishers Ltd.: London, 1988; Chapter 3.

DOI: 10.1021/acs.macromol.5b02419
Macromolecules 2016, 49, 2228−2237